Wood Sci Technol (2016) 50:807–832
DOI 10.1007/s00226-016-0810-8

ORIGINAL

Eigenproblems in timber structural elements with uncertain properties

Diego A. García[1,2,3] · Rubens Sampaio[4] · Marta B. Rosales[1,3]

Received: 10 February 2015 / Published online: 16 March 2016

Abstract A stochastic model of sawn timber structural elements of Argentinean *Eucalyptus grandis* is applied to the study of two eigenproblems. One is the free vibrations problem which, after being solved, yields the natural frequencies and modes. The other problem is the buckling of columns. Its solution leads to the buckling loads and modes. The governing differential equations are stated starting from the Euler–Bernoulli beam theory. Then, they are discretized and numerically approximated through the finite element method. The stochasticity is given by the mechanical properties involved in each problem. The lengthwise variabilities of the modulus of elasticity and of the second moment of the cross-sectional area are simulated to account for the presence of knots. The variability of the mass density among structural elements is also considered. The statistics of the solutions are obtained. The probability density functions of the natural frequencies and the buckling loads are numerically obtained through a stochastic finite element concept using Monte Carlo simulation. Numerical results for the first natural frequency are validated with experimental values. The mode shape statistics are also analyzed. Frequently the presence of knots in sawn timber structures is disregarded, usually due to the lack of data and the availability of an adequate representation. The model herein presented contributes to attain a more realistic description of structures made

✉ Diego A. García
garciadiego@fio.unam.edu.ar; diegoalbertogarcia@outlook.com

[1] Department of Engineering, Universidad Nacional del Sur, Av. Alem 1253, 8000 Bahía Blanca, Argentina

[2] Department of Civil Engineering, Universidad Nacional de Misiones, Juan Manuel de Rosas 325, 3360 Oberá, Argentina

[3] CONICET, Bahía Blanca, Argentina

[4] Department of Mechanical Engineering, Pontifícia Universidade Católica do Rio de Janeiro, Rua Marquês de São Vicente, 225, Rio de Janeiro, RJ 22453-900, Brazil

out of sawn timber due to the unavoidable variability of the properties, in particular the presence of knots.

Introduction

The design of structures should satisfy two main requirements. The first one is safety, usually expressed in terms of a certain load bearing capacity. The second requirement is the serviceability, which refers to the ability of the structural system to perform satisfactorily in normal use. One of the serviceability requirements is related to the dynamic behavior of the structural systems and elements. Moreover, the load bearing capacity can be reduced when the compressive load approaches the buckling limit. Structural standards define limit values of the natural frequencies in order to control the dynamic behavior of timber floors, bridges and frames and also limit values of the compressive loads in order to avoid buckling. In this work, these two structural problems, represented mathematically as eigenproblems, are addressed through the study of the dynamic behavior of beams and the buckling problem in columns of Argentinean *Eucalyptus grandis* sawn structural elements with uncertain properties.

Argentinean *Eucalyptus grandis* is one of the most important renewable species cultivated in Argentina (INTA 1995). A simple method for visually strength grading sawn timber of these species has been developed by Piter et al. (2004). As reported in this paper, the presence of pith and knots is considered the most important visual characteristic for strength grading this material by the Argentinean standard IRAM 9662-2 (2006).

Due to its natural origin, structural timber is characterized by considerable lengthwise variability of its mechanical properties. However, these properties are usually treated as random variables and their spatial variability is not explicitly taken into account in the design practice. Growth defects such as knots, often related to localized grain deviations, are the main source of the lengthwise variability of bending strength and stiffness in sawn beams. It is apparent that a stochastic approach becomes necessary in order to attain a more realistic structural model.

The stochastic approaches employed for the modeling of the mechanical properties of timber are derived from the probabilistic theories of random variables and processes. They allow simulating the timber mechanical properties with the objective to perform the structural analysis. The lengthwise variation of the modulus of elasticity (MOE) was modeled by Kline et al. (1986) with a second-order Markov model. This method was applied in order to generate serially correlated MOE values along segments for a piece of lumber. The influence of the knots in the structural behavior of timber beams was considered by Czmoch (1998). He studied the bending strength in sections with knots and determined the load carrying capacity of timber beams modeling the presence of knots through a Poisson process. He also assumed the MOE variation as a stationary Gaussian random field simulated through the Nataf transformation. Köhler et al. (2007) presented a probabilistic model of timber structures where the MOE is represented as a random variable with a lognormal PDF, assuming a homogeneous value within a structural element.

Köhler (2007) reported a model of the lengthwise variability of the bending strength, following the weak-zone approach proposed by Isaksson (1999) for the bending moment capacity, in which the discrete section transition was assumed to be Poisson distributed. In the weak-zone model, the structural timber is modeled as a composite of weak zones connected by sections of clear wood.

Several works have studied the influence of the timber knots in the performance of structural elements through the finite element method (FEM). Baño et al. (2011) presented a study in which they simulated timber beams with defects and predict their maximum load in bending. The model was implemented in a FE software. Baño et al. (2012) reported in a study regarding the development of a bi-dimensional model of timber pieces free of defects in order to predict the performance of timber structural elements. The influence of the size and position of cylindrical knots on the load capacity of timber elements using a FE program was analyzed by Baño et al. (2013). Guindos and Guaita (2013) studied a three-dimensional wood material model implemented in a finite element software capable of predicting the behavior of timber at the macroscale taking into account the effect of any type of knot. Then, Guindos and Guaita (2014) assessed the influence of different types of knots and the fiber deviations on the bending of wood elements, using visual grading standards. A finite element simulation tool which is able to consider a realistic three-dimensional fiber course in the vicinity of knots was presented by Lukacevic and Füssl (2014). The knots are modeled as rotationally symmetric cones with their apexes lying on a piecewise linear pith.

The well-known FEM and the stochastic tools are combined in the stochastic finite element method (SFEM). Der Kiureghian and Ke (1988) used the SFEM and applied it to structural reliability studies. Among other results, the authors studied the relationship between the finite element and the correlation lengths of the random field in order to obtain a good representation of the material properties variability with random field discretized with the midpoint method. The random system parameters were modeled as second-order stochastic processes defined by their mean and covariance functions by Ghanem and Spanos (1991) in their book about SFEM. The Karhunen–Loève expansion was used to represent these processes in terms of a countable set of uncorrelated random variables.

Various authors have presented transformation techniques in order to simulate random variables applied to reliability studies. Der Kiureghian and Liu (1986) introduced the Nataf transformation and applied it to structural reliability under incomplete probability information of the random variables. If only marginal PDFs and correlation data are available, even for non-normal random variables, the Nataf transformation can be applied to give a set of independent normal random variables. Ditlevsen and Madsen (1996) and Melchers (1999) dealt, respectively, with this transformation in their books in reliability methods together with others approaches such as the Rosenblatt transformation.

Tools such as the principle of maximum entropy (PME) proposed by Shannon (1948) and the well-known Monte Carlo simulation (MCS) approach (Rubinstein and Kroese 2007) are commonly employed in numerical stochastic studies. The PME allows establishing the PDF of a random variable that best represents the state of knowledge about it.

In the present work, a stochastic model of timber sawn structural elements of Argentinean *Eucalyptus grandis* is presented. This model is employed for the study of the eigenproblems. From these, the first three natural frequencies and buckling loads, and the corresponding mode shapes are obtained. The differential equations are formulated starting from the Euler–Bernoulli (E–B) beam theory, and then, they are discretized and numerically approximated through the FEM. The lengthwise variability of the MOE and the second moment of area account for the knots presence. For the first parameter, the local reduction of the MOE due to the grain deviation produced by the knot presence is considered. The lengthwise variability of the MOE presented in this work was developed starting from the weak-zone model with modifications in the length of this zone. For the second moment of area, the timber knot parameters are modeled via the joint probability mass function (JPMF) obtained with experimental data from visual survey of beams. This method is different to those frequently used in order to study the knots influence. Frequently they are introduced in a deterministic context with fixed location and size. In this study, timber knots are modeled as holes in the cross section, hence considered in the second moment of area of the element cross section. The mass density is considered constant along the beam span and the lengthwise variability due to the knot presence is not taken into account. In the timber structural elements of this species, the knots are frequently composed of material with similar density to the clean wood. In order to simulate the mass in the inertial term, the PDF of this parameter was obtained. Through MCS, the PDFs of the first three natural frequencies and buckling loads are obtained. For the validation of the numerical results, a comparison is made with experimental values of the first natural vibration frequency. Then, the influence in the structural response of each of the stochastic parameters is studied and analyzed. From this analysis, the vibration and buckling modes are studied as stochastic processes.

The stochastic model presented in this work provides good predictions of the structural behavior of sawn elements of Argentinean *Eucalyptus grandis*. The stochastic analysis allows to obtain a higher range of results than a deterministic study, and the influence of the mechanical properties in the results is better understood.

Materials and methods

This study presents eigenproblems of pinned-pinned sawn structural elements of Argentinean *Eucalyptus grandis* with knots according to the E–B beam theory. For the free vibration problem of a simply supported beam, the well-known differential equation is the following:

$$\rho(x)a(x)\frac{\partial^2 v(x,t)}{\partial t^2}+\frac{\partial^2}{\partial x^2}\left(e(x)i(x)\frac{\partial^2 v(x,t)}{\partial x^2}\right)=0 \tag{1}$$

where $\rho(x)$ is the material density per unit length; $a(x)$ is the area of the beam cross section; $e(x)$ is the MOE; $i(x)$ is the second moment of the beam cross section with respect to the z axis; $v(x, t)$ is the transverse displacement; x is the position along the

beam length; and t is the time. For the static buckling problem, the time variable disappears and the deflection field $v(x)$ and the buckling load p_{cr} are related by the following equation:

$$\frac{\mathrm{d}^2}{\mathrm{d}x^2}\left(e(x)i(x)\frac{\mathrm{d}^2v(x)}{\mathrm{d}x^2}\right) - p_{cr}\frac{\mathrm{d}^2}{\mathrm{d}x^2}(v(x)) = 0. \tag{2}$$

In the present work, the lengthwise variabilities of the MOE and of the second moment of area of the beam cross section are introduced due to the presence of timber knots that produces a local reduction of both. Random variables are used for this purpose, and in what follows, these stochastic quantities are denoted by capital letters. The differential equations, Eqs. (1) and (2), respectively, become:

$$Pa\frac{\partial^2V(x,t)}{\partial t^2} + \frac{\partial^2}{\partial x^2}\left(E(x)I(x)\frac{\partial^2V(x,t)}{\partial x^2}\right) = 0 \tag{3}$$

$$\frac{\mathrm{d}^2}{\mathrm{d}x^2}\left(E(x)I(x)\frac{\mathrm{d}^2V(x)}{\mathrm{d}x^2}\right) - P_{cr}\frac{\mathrm{d}^2}{\mathrm{d}x^2}(V(x)) = 0. \tag{4}$$

In this study, timber knots are modeled as holes along the beam that modify the second moment of area of the beam cross section and consequently the bending stiffness. However, no holes are considered in the mass since the knots mass participates in the inertial terms disregarding an eventual density change. The variation of the mass density P among the beams of the sample is considered.

Finite elements discretization

Let us state the variational formulation prescribing a set of admissible functions ψ:

$$\int_0^L \left[\rho(x)a(x)\frac{\partial^2v(x,t)}{\partial t^2} + \frac{\partial^2}{\partial x^2}\left(e(x)i(x)\frac{\partial^2v(x,t)}{\partial x^2}\right)\right]\phi(x)\mathrm{d}x = 0 \qquad \forall\phi\in\psi \tag{5}$$

$$\int_0^L \left[\frac{\mathrm{d}^2}{\mathrm{d}x^2}\left(e(x)i(x)\frac{\mathrm{d}^2v(x)}{\mathrm{d}x^2}\right) - p_{cr}\frac{\mathrm{d}^2}{\mathrm{d}x^2}(v(x))\right]\phi(x)dx = 0. \qquad \forall\phi\in\psi \tag{6}$$

For the pinned-pinned problem,

$$\psi = \{\phi : [0,L]\to\mathbb{R}, \phi \text{ is piecewise } \mathcal{C}^2 \text{ and bounded}, \phi(0) = 0, \phi(L) = 0\}. \tag{7}$$

This formulation, together with the boundary conditions, conduces to the following form of the two variational problems:

$$M(v,\phi) + K(v,\phi) = 0 \qquad \forall\phi\in\psi \tag{8}$$

$$K(v,\phi) = p_{cr}K^G(v,\phi) \qquad \forall\phi\in\psi \tag{9}$$

where, from Eq. (8), $M(v,\phi)$ and $K(v,\phi)$ are the mass and stiffness operators, respectively, defined as follows:

$$M(v,\phi) = \int_0^L \rho(x)a(x)\frac{\partial^2 v(x,t)}{\partial t^2}\phi(x)\mathrm{d}x$$
$$K(v,\phi) = \int_0^L e(x)i(x)\frac{\partial^2 v(x,t)}{\partial x^2}\frac{\partial^2 \phi(x)}{\partial x^2}\mathrm{d}x \tag{10}$$

and, from Eq. (9), $K(v,\phi)$ and $K^G(v,\phi)$ are the stiffness and geometrical stiffness operators, respectively, defined as follows:

$$K(v,\phi) = \int_0^L e(x)i(x)\frac{\mathrm{d}^2 v(x)}{\mathrm{d}x^2}\frac{\mathrm{d}^2 \phi(x)}{\mathrm{d}x^2}\mathrm{d}x$$
$$K^G(v,\phi) = \int_0^L \frac{\mathrm{d}v(x)}{\mathrm{d}x}\frac{\mathrm{d}\phi(x)}{\mathrm{d}x}\mathrm{d}x \tag{11}$$

Equations (8) and (9) are numerically approximated using the Galerkin method. A N-dimensional subspace $\psi^N \subset \psi$ is defined and approximating functions $v^N \in \psi^N$ are searched for. The variational problems can be formulated as follows: Find $v^N \in \psi^N$ such that:

$$M(v^N,\phi) + K(v^N,\phi) = 0 \qquad \forall\phi \in \psi^N \tag{12}$$

$$K(v^N,\phi) = \hat{p}_{cr}K^G(v^N,\phi) \qquad \forall\phi \in \psi^N \tag{13}$$

Applying the standard finite element methodology (e.g., Bathe 1982) the variational forms, Eqs. (12) and (13) are discretized. Euler-Bernoulli beam elements with two nodes and two degrees of freedom per node (transverse displacement and rotation, respectively) are employed. *Hermitian* shape functions are considered for spatial interpolation of the transverse deflection $v(x)$, in terms of the nodal variables.

$$v(x) = n_1(x)v_1 + n_2(x)\theta_1 + n_3(x)v_2 + n_4(x)\theta_2 \tag{14}$$

where

$$n_1(x) = 1 - \frac{3x^2}{{L_e}^2} + \frac{2x^3}{{L_e}^3} \qquad n_3(x) = \frac{3x^2}{{L_e}^2} - \frac{2x^3}{{L_e}^3}$$
$$n_2(x) = x - \frac{2x^2}{L_e} + \frac{x^3}{{L_e}^2} \qquad n_4(x) = -\frac{x^2}{L_e} + \frac{x^3}{{L_e}^2}$$

and L_e is the element length.

The application of *Hermitian* shape functions and the Galerkin's method to Eq. (10) results in the stiffness matrix and the mass matrix of the beam element. The elements of these matrices are, respectively:

$$K_{e,ij} = \int_0^{L_e} E(x)I(x)\frac{d^2 n_i(x)}{\mathrm{d}x^2}\frac{\mathrm{d}^2 n_j(x)}{\mathrm{d}x^2}\mathrm{d}x$$
$$M_{e,ij} = Pa\int_0^{L_e} n_i(x)n_j(x)\mathrm{d}x \tag{15}$$

and Eq. (11) yields the stiffness matrix and the geometrical stiffness matrix of the beam element. The elements of these matrices are, respectively:

$$K_{e,ij} = \int_0^{L_e} E(x)I(x)\frac{\mathrm{d}^2 n_i(x)}{\mathrm{d}x^2}\frac{\mathrm{d}^2 n_j(x)}{\mathrm{d}x^2}\mathrm{d}x$$
$$K^G_{e,ij} = \int_0^{L_e} \frac{\mathrm{d}n_i(x)}{\mathrm{d}x}\frac{\mathrm{d}n_j(x)}{\mathrm{d}x}\mathrm{d}x \tag{16}$$

where the random quantities $E(x)$ and $I(x)$ represent the lengthwise variability along the beam. P is the mass density random variable which changes among beams, though its lengthwise variability is not taken into account within each beam.

Next, the global stiffness matrix, the mass matrix and the geometrical stiffness matrix can be obtained with the usual finite element assembling. The natural frequencies and modes are obtained solving the next equation:

$$[\mathbf{K} - \Omega_n^2\mathbf{M}]\Phi_n = 0 \tag{17}$$

where $\mathbf{K}$ and $\mathbf{M}$ are the $n \times n$ positive-definite global stiffness and mass matrices, respectively, Ω_n is the nth natural circular frequency and Φ_n is the associated natural vibration mode.

The buckling load is obtained solving the following equation:

$$\mathbf{K} - \hat{p}_{cr}\mathbf{K^G} = 0 \tag{18}$$

where $\mathbf{K}$ and $\mathbf{K^G}$ are the $n \times n$ positive-definite global stiffness and geometrical stiffness matrices of elements in compression, respectively, and $\hat{p}_{cr}$ is the buckling load.

Mechanical properties of the models

This section presents the assumptions and the way in which the mechanical properties that appear in Eqs. (3) and (4) are represented.

Random field of the Second Moment of Area: Timber knots geometric parameters

In order to simulate the timber knots, the joint probability mass function (PMF) of the timber knot shape parameters (O, Q, R) within the structural element cross section is defined. The probability mass functions of the distance between timber knots (U) and of its length (W) in the direction parallel to the longitudinal axis of the structural element are also stated. To find the joint PMF of the knots parameters, experimental data obtained from a visual survey of 25 sawn beams of *Eucalyptus grandis* of structural size with 180 timber knots were employed. The nominal section of the beams employed in the visual survey is 50 mm × 150 mm and 3 m of length. The distance between knots, their dimensions perpendicular and parallel to the longitudinal beam axis, their depth and position within the beam cross section are the knot features reported in the visual survey.

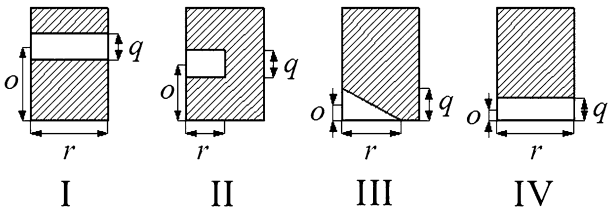

Fig. 1 Knots shapes classification and variables considered in the joint probability mass function (PMF)

Considering these visual parameters, the timber knots were classified into four types (Fig. 1):

I. Timber knots with the depth equal to the structural element width and with vertical position along the structural element height.
II. Timber knots with the depth less than the structural element width and with vertical position along the structural element height.
III. Timber knots with the depth less than the structural element width and with vertical position near to the edge of the structural element cross section.
IV. Timber knots with the depth equal to the structural element width and with vertical position near to the edge of the structural element cross section.

Taking into account the parameters that define the position and dimensional characteristic of the timber knots within the structural element cross section, the joint PMF of the three random variables is defined in order to simulate the dimensions of the timber knots and their position within the structural element cross section:

$$\begin{aligned} p_{O,Q,R}(o,q,r) &= p_R(r \mid o,q)p_Q(q \mid o)p_O(o) \\ &= P[R = r \mid O = o, Q = q]P[Q = q \mid O = o]P[O = o] \end{aligned} \tag{19}$$

where the random variables and their statistics values are (see Fig. 1 and recalling that capital letters denote random variables):

- O is the position of the knot centroid along the height of the structural element cross section. Mean value μ = 61.62 mm and standard deviation SD σ = 38.77 mm. The sample space ranges from 10 to 136 mm.
- Q is the knot height (dimension perpendicular to the longitudinal structural element axis). Mean value μ = 23.95 mm and SD σ = 11.46 mm. The sample space ranges from 5 to 50 mm.
- R is the knot depth along the width of the structural element cross section. Mean value μ = 20.22 mm and SD σ = 11.49 mm.

In the type II knots, the timber beams of the visual survey are not cut through the cross section with the knot after the experimental test to determine their depth r because they become useless to perform other tests. Due to the lack of information

about this random variable, the principle of maximum entropy (PME) (Shannon 1948) is applied to obtain the probability distribution of R. The PME states that, subjected to known constrains, the joint PMF which best represents the current state of knowledge is the one with largest entropy. The measure of uncertainties of a discrete random variable R is defined by the following expression:

$$S(p) = -\sum_{i=1}^{n} p_i \ln(p_i) \tag{20}$$

where S is the entropy of the random variable and p_i is the probability of the discrete random variable R which assumes n different values. It is possible to demonstrate that the application of the PME, when the random variable assumes a finite number of values within the interval $[a, b]$ and no further information about the random variable is known, leads to a uniform PMF.

The random variables that define the distance between timber knots and their dimensions in the direction parallel to the structural element axis are, respectively:

- U is the distance among timber knots. Mean value μ = 288.62 mm and SD σ = 175.52 mm. The sample space ranges from 15 to 1040 mm.
- W is the length of the knot (dimension along the longitudinal structural element axis). Mean value μ = 40.19 mm and SD σ = 21.36 mm. The sample space ranges from 8 to 105 mm.

The dimension of the knot in the direction parallel to the longitudinal structural element axis w is related to the dimension in the direction perpendicular to the axis named q. These random variables are defined by the joint PMF $p_{Q,W}(q, w)$. The random variable U is considered independent from the other ones due to the fact that there is no strong evidence of the relation between the position of the knots along the beams and their geometry variables.

In order to validate the numerical model with the experimental data, and since the knots geometry is discrete, the PMFs are a natural choice. Given that the density of the data is considered enough to represent adequately the statistics of the random variables, the use of this type of distribution is extended to the whole study.

Random field of the Modulus of Elasticity (MOE)

The MOE values in this model are assigned as a function of the knot ratio (K) of each knot or knots clusters. The knot dimension is calculated as the distance between two tangents to the knot, parallel to the beam axis. Let us denote by k_1 the knot dimension if the knot is isolated, i.e., separated of the next knot in a distance larger than the cross-sectional height. In the case this distance is smaller, a knots cluster is defined including these knots. The length of this region is assumed as the cross-sectional height. Then, k_2 states for the sum of all the dimensions of the knots grouped in the cluster. The knot ratio (K) is calculated as k_1/k_3 or k_2/k_3, depending on the situation. This knot ratio is adopted from the visual strength grading presented in the Argentinean norm IRAM 9662-2 (2006).

In the beam sections with K equal to zero (i.e., free-of-knots sections), the MOE values are assigned through the Nataf transformation. In the beam sections with K different from zero (sections with knots), the MOE values are uncorrelated random variables assigned through their marginal probability density function (PDF) defined for each value of K.

The present approach is similar to the weak-zone model proposed by Isaksson (1999), but unlike this work, it considers the lengthwise variability of the MOE in the sections without knots. In the weak-zone model, the structural timber component is modeled as a composite of short weak zones connected by longer sections of clear wood. The length of the weak zones is proportional to five times the largest knot dimension (q, w). This feature was observed in the visual survey of the timber knots and the surrounding fibers. The MOE in each of these zones is constant and randomly assigned.

MOE in free-of-knots sections: Nataf transformation

The Nataf transformation is employed in order to generate and simulate the random field of the MOE. Introduced by Der Kiureghian and Liu (1986), it allows to build a multidimensional PDF that fits a prescribed marginal distributions and a correlation matrix. Suppose that a random vector X has prescribed marginal distributions, say $F_{X_i}(X_i)$, $i = 1, \ldots, M$ and the correlation matrix $\mathbf{R}$. It is possible to transform the components of $\mathbf{X}$ into standard normal random variables ξ_i, $i = 1, \ldots, M$, as follows:

$$\xi_i = \Phi^{-1}(F_{X_i}(x_i)) \tag{21}$$

The Nataf transformation assumes that $\boldsymbol{\Xi} = \{\Xi_1, \ldots, \Xi_M\}^T$ is a standard normal correlated vector which joint PDF is the multidimensional normal PDF $\varphi_M(\boldsymbol{\xi}; \mathbf{R_0})$:

$$\varphi_M(\boldsymbol{\xi}; \mathbf{R_0}) = \frac{1}{\sqrt{(2\pi)^M \det \mathbf{R_0}}} \exp\left[-\frac{1}{2}\boldsymbol{\xi}^T \mathbf{R_0}^{-1} \boldsymbol{\xi}\right] \tag{22}$$

and R_0 is a correlation matrix (corresponding to the multidimensional normal PDF) that should be compatible with the prescribed correlation matrix R (corresponding to the random field of the prescribed marginal distribution). From the above equations, one can write:

$$f_{\mathbf{X}}(x_1, \ldots, x_M) = f_{\boldsymbol{\Xi}}(\xi_1, \ldots, \xi_M)\left|\det \mathbf{J}_{\boldsymbol{\Xi},\mathbf{X}}\right| \tag{23}$$

where the Jacobian of the transform $\mathbf{J}_{\boldsymbol{\Xi},\mathbf{X}}$ is a diagonal matrix with elements $f_{X_i}(x_i)/\varphi(\xi_i)$, $i = 1, \ldots, M$. This leads to the Nataf transformation

$$f_{\mathbf{X}}(x_1, \ldots, x_M) = \prod_{i=1}^{M} \frac{f_{X_i}(x_i)}{\varphi(\xi_i)} \varphi_M(\boldsymbol{\xi}; \mathbf{R_0}) \tag{24}$$

The correlation matrix $\mathbf{R_0}$ is computed term by term by solving the following consistency equation for ρ_{ij}:

$$\rho_{ij} = \int_{-\infty}^{\infty}\int_{-\infty}^{\infty}\left(\frac{x_i - \mu_{X_i}}{\sigma_{X_i}}\right)\left(\frac{x_j - \mu_{X_j}}{\sigma_{X_j}}\right)\varphi_2(\xi_i, \xi_j; \rho_{0ij})d\xi_i d\xi_j \tag{25}$$

where ρ_{ij} and ρ_{0ij} are the non-dimensional correlation matrix elements of $\mathbf{R}$ and $\mathbf{R_0}$, respectively. For given marginals and correlation coefficients ρ_{ij} of two variables X_i and X_j, the preceding equation can be solved iteratively to find ρ_{0ij}. To avoid such tedious calculations, a set of semiempirical formulas of the ratio $F = \rho_{0ij}/\rho_{ij}$ have been tabulated for various pairs of distributions $(f_{X_i}(x_i), f_{X_j}(x_j))$ in Der Kiureghian and Liu (1986), Ditlevsen and Madsen (1996) and Melchers (1999). In the present work, $f_{X_i}(x_i)$ and $f_{X_j}(x_j)$ are assumed to be gamma distributed. Hence, the value of F is defined as:

$$\begin{aligned} F = \frac{\rho_{0ij}}{\rho_{ij}} =& 1.022 + 0.022\rho_{ij} - 0.012(\delta_i + \delta_j) + 0.001\rho_{ij}^2 + 0.125(\delta_i^2 + \delta_j^2) \\ & -0.077\rho_{ij}(\delta_i + \delta_j) + 0.014\delta_i\delta_j \end{aligned} \tag{26}$$

where δ_i and δ_j are the coefficients of variation. Here, it has been assumed that $\delta_i = \delta_j$. This assumption is based on the properties of the simulated random field which is homogeneous and stationary. This last statement was also adopted in Kline et al. (1986) and Czmoch (1998). A good agreement with experimental results is shown in the last reference.

The correlation structure of the random field is described by means of the correlation function. An exponential correlation function, proposed by Czmoch (1998), based on experimental test carried out on pine–spruce beams grade K24 according to the Swedish standard SBN 1980 (1981) is assumed:

$$\rho_{ij} = \exp\left(-2\frac{\left|x_c^{(j)} - x_c^{(i)}\right|}{d}\right) \tag{27}$$

where d is the correlation length which measures the decay of the correlation function. In this work, the values considered for the correlation length of the MOE random field are d =1.34 m (named d_1) and $d \to \infty$ (named d_∞). When $d \to \infty$, the random field becomes fully correlated and the random field can be interpreted as a random variable in the limit. It represents a beam with homogeneous MOE though random; i.e., it changes from one beam to the other randomly. This second case is often used in reliability studies and in design practice. Czmoch (1998) experimentally found that the correlation length of the MOE for pine–spruce beams is approximately 1.4 m for the serviceability load level and around 0.7 m for a load level close to the load carrying capacity. These values of correlation length were determined in beams with dimensions and load levels analogous to those employed in the following sections of the present study. The *Eucalyptus grandis* cultivated in the Mesopotamian provinces of Argentina has a very high ratio MOE/density higher than all covered in the standard EN 338 (1996) for deciduous species, according to the results of the investigation performed by Piter (2003). This feature, which can be a particular advantage for the structural use of the material, indicates a behavior

similar to the coniferous species. In García et al. (2013), a validation with different values of the correlation length found within the above established interval was presented. It was found that the validation with experimental results of static deflections was best attained with the correlation length d_1 adopted herein.

Marginal PDF of the MOE

In order to determine the marginal PDF of the MOE, the PME for a continuous random variable is applied (cf the previous case for a discrete random variable Eq. 20). The measure of uncertainties of the continuous random variable X is defined by the following expression

$$S(f_X) = -\int_D f_X(x)\ln(f_X(x))\mathrm{d}x \tag{28}$$

where f_X stands for the PDF of the random variable X and D is its domain. It is possible to demonstrate that the application of the principle under the constraints of positiveness and bounded second moment leads to a gamma PDF. The PME conduces to this PDF due to the fact that the domain of the MOE is real and positive. The known constraints of the continuous random variable that represents the MOE are:

$$\int_0^\infty f_X\mathrm{d}x = 1 \qquad E[X] = \mu_X < \infty \qquad E[\ln(X)] < \infty \tag{29}$$

To find the parameters of the marginal PDF of the MOE, experimental data presented by Piter (2003) are employed. These values were obtained by means of two point load bending tests, performed with 349 sawn beams of Argentinean *Eucalyptus grandis* with structural dimensions. Bending tests were carried out according to the standard EN 408 (1996).

The parameters of the gamma marginal PDF of the MOE are estimated with the help of the maximum likelihood method (MLM). Then, the test of fit Kolmogorov–Smirnov (K–S) is used (e.g., Benjamin and Cornell 1970). The PDF that best fits with the experimental values is the gamma, in agreement with the PME. The test of fit was also carried out with the lognormal and normal PDFs, the first one since Köhler et al. (2007) proposed it to model the MOE and the second PDF as it is often employed to represent mechanical properties. The normal PDF fits the experimental data best. However, the use of this PDF in the model would occasionally lead to negative values of the MOE which are physically unacceptable. Thus, the gamma and lognormal PDF seem more suitable. The gamma marginal PDF and CDF of the MOE are, respectively:

$$f(x \mid a,b) = \frac{1}{b^a\Gamma(a)}x^{a-1}e^{-\frac{x}{b}} \qquad F(x \mid a,b) = \frac{1}{b^a\Gamma(a)}\int_0^x t^{a-1}e^{-\frac{t}{b}}\mathrm{d}t \tag{30}$$

where a and b denote the shape and scale parameters, respectively. In Table 1, the marginal PDFs of the MOE for each value of K are presented.

Table 1 Parameters of the gamma marginal PDF of the MOE for each value of K

Parameters	$E(x) \rightarrow K = 0$	$E_i \rightarrow 0 < K \leq 1/3$	$E_i \rightarrow 1/3 < K \leq 2/3$	$E_i \rightarrow 2/3 < K$
a	31.301	42.730	35.370	35.464
b	0.508	0.315	0.364	0.328
μ (GPa)	15.89	13.46	12.87	11.63
σ (GPa)	2.83	2.06	2.16	1.95
$\delta = \sigma/\mu$	0.18	0.15	0.17	0.17

Mass density

In this work, the mass density in the simply supported sawn beams of Argentinean *Eucalyptus grandis* is considered constant along the beam span and the lengthwise variability due to the knot presence is not taken into account. In the timber structural elements of this species, the knots are frequently composed of material with similar density to the clear wood. This does not mean that the mass lengthwise variability would not be present in timber structural elements, but this feature is not considered in this paper.

The variability in the density among beams is considered through the PDF. In order to determine the marginal PDF of the mass density, the PME for a continuous random variable is applied, like the previous case. The application of the principle under the constraints of positiveness and bounded second moment leads to a gamma PDF. The PME conduces to this PDF due to the fact that the domain of the mass density is real and positive. To find the parameters of the PDF of the random variable mass density (P), experimental data presented by Piter (2003), obtained by means of density measurements performed with 349 sawn beams of Argentinean *Eucalyptus grandis*, are employed. The density measurements were carried out according to EN 408 (1996).

Köhler (2007) represented the variability of the mass density among structural timber beams with a normal PDF for European softwood species. In the present work, the parameters of the PDF of the mass density are estimated with the help of the MLM. Finally, the K–S test of fit is used to choose the PDF that fits best. As before, assuming $\alpha = 0.05$, the critical value for the K–S test of fit is equal to c = 1.36. The K–S statistics are the following: lognormal 0.65, gamma 0.69 and normal 0.75. As can be seen, the three PDFs fulfill the critical value, but the lognormal and gamma fit best with respect to the experimental values. Here, following the PME and due to the small difference found among the lognormal and gamma, the latter is adopted in order to introduce the mass density uncertainty in the stochastic model. The gamma PDF and CDF of the mass density P are, respectively:

$$f(x \mid a, b) = \frac{1}{b^a \Gamma(a)} x^{a-1} e^{-\frac{x}{b}} \qquad F(x \mid a, b) = \frac{1}{b^a \Gamma(a)} \int_0^x t^{a-1} e^{-\frac{t}{b}} \mathrm{d}t \tag{31}$$

where $a = 72.179$ and $b = 7.659$ denote the shape and scale parameters, respectively. The correlation coefficient between the values of the MOE and the density is 0.5. In Köhler et al. (2007), a correlation coefficient of 0.6 for European softwood was

presented. According to the above-mentioned work, the correlation coefficient shows a medium/low level of correlation among these parameters. Piter (2003) remarks that it is not possible to find differences in the density values between the two best strength classes of *Eucalyptus grandis* timber, according to the visual grade classification presented in his work, for practical purposes, while both classes exhibit small variations from the third one. This visual grade classification is slightly amended and then it is adopted by the standard IRAM 9662-2 (2006). The Argentinean standard CIRSOC 601 (2013) follows this suggestion and adopts a unique value of mass density for the considered qualities of structural timber and applied to verify the serviceability conditions. Taking into account the above-mentioned assumptions and studies about the relationship between the MOE and the mass density, these random variables are assumed to be uncorrelated within this study.

Results and discussion

Natural vibration modal analysis

Numerical results of the first three natural frequencies F_n and modes Φ_{Fn} of pinned-pinned *Eucalyptus grandis* timber beams are reported in this section. In all the FEM simulations, 100 beam elements are analyzed. The integrals of the components of the element stiffness matrix (Eq. 15) are computed by means of the Gauss quadrature using five points. The dimensional parameters of the timber knots are simulated with the inverse transform method (Rubinstein and Kroese 2007). The dimensional parameters of the timber beams employed in the numerical simulation are the following: a length of 3 m and a nominal section of the beam of 50 mm x 150 mm. These dimensional parameters correspond to timber beams of structural size, which are often employed in design practice.

A convergence study was carried out varying the number of independent MCS *ns* and evaluating the results of $E[F_1]$ (the mean value of the first natural frequency). The graphic results are not shown herein for brevity. The adopted convergence criterion was the following: $|E[F_1^{ns}] - E[F_1^{ns-200}]| \leq 0.1$ Hz, where $E[F_1^{ns}]$ is the mean value of the first natural frequency for a number of simulations *ns* and $E[F_1^{ns-200}]$ is the mean value of the first natural frequency for a number of simulations $ns - 200$. The probabilistic model for d_∞ showed higher values of $E[F_1]$ than for the same model for d_1, and the plots of the mean value variation with respect to *ns* are more separated. This study was carried out in order to determine the appropriate number of simulations to attain a prescribed accuracy.

Validation of the stochastic model

In this section, a comparison between numerical and physical experiments through the analysis of the first natural frequency is presented. Experimental data, obtained by means of the test presented in Piter (2003) performed with 50 sawn beams of

Argentinean *Eucalyptus grandis* with a nominal section of 50 mm × 150 mm and a length of 3 m, are employed. The fundamental frequency of vibration was obtained mechanically exciting the beams through an impact at one end and placing the sensor in the center of the body, in the antinodal position.

The comparison of the cumulative distribution function (CDF) of the first natural frequency found with numerical and experimental approaches is shown in Fig. 2. Numerical results correspond to two different values of the weak-zone length. The first plot was obtained with a weak-zone length equal to five times the major knot dimension (5 max (q, w)), while the second plot corresponds to a weak-zone length equal to seven times the major knot dimension (7 max(q, w)). The numerical and experimental results for the two values of the weak-zone length were compared. Numerical results for the first case (5 max (q, w)) and d_1 are acceptable and show a good prediction of the first natural frequency of the tested beams. The statistics obtained from the experimental results are the following: mean value $E[F_1] = 77.33$ Hz and SD $\sigma[F_1] = 5.03$ Hz. Meanwhile, the statistical values obtained from the numerical results with a weak-zone length equal to 5 max(q, w) and the correlation length d_1 are the following: mean value $E[F_1] = 76.47$ Hz and SD $\sigma[F_1] = 6.66$ Hz. The mean values numerically obtained are close to the experimental ones while the SD and coefficients of variation present higher values with respect to the experimental results.

In addition, the dynamic properties calculated from each tested beam (constant within the beam span) were included in the numerical model and this case is named homogeneous with experimental properties (HEP). The results are shown in the same figure. In the engineering practice, timber properties are generally considered constant along the element, and this assumption would lead to over or under evaluation of the dynamic response. The objective of the stochastic model herein proposed is to obtain a more realistic material approach and a better understanding of the influence of the timber mechanical and physical properties in the structural behavior.

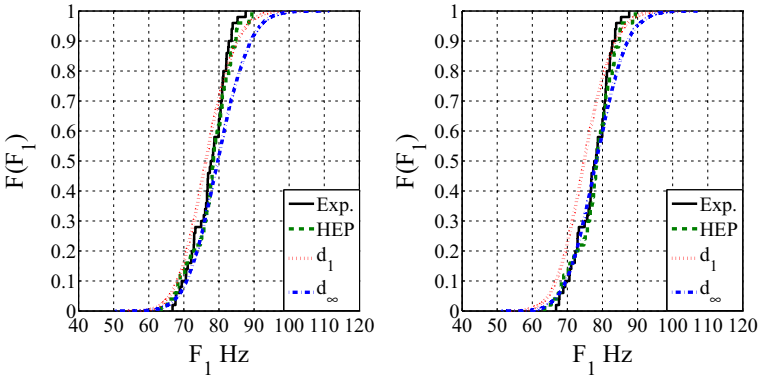

Fig. 2 Fundamental frequency. Comparison between numerical and experimental results CDF of F_1 for two different weak-zone lengths, *left plot* five times the major knot dimension and *right plot* seven times the major knot dimension

Influence of the random field I(x) in the natural frequencies

The influence of the random field $I(x)$ due to the knots presence in the first three natural frequencies F_n is studied herein. To accomplish this, the MOE and the mass density are supposed to assume a deterministic constant value along the beam. Thus, the only uncertainty source is the random field of the second moment of area. The adopted reference values are the following: $E_0 = 15.89$ GPa, $\rho_0 = 552.86$ kg/m^3, $I_0 = 9.542\times10^{-6}$ m^4 and $A_0 = 0.0058$ m^2. The value of I_0 corresponds to a beam without knots. For these reference values and a beam length $L = 3$ m, the first three natural frequencies obtained through the classical equation for a simply supported beam with homogeneous properties ($f_n = (n^2\pi/2L^2)\sqrt{(E_0 I_0)/(A_0\rho_0)}$) are $F_{01} = 37.95$ Hz, $F_{02} = 151.80$ Hz and $F_{03} = 341.56$ Hz, respectively. In Fig. 3, the PDFs of the first three natural frequencies obtained through the application of MCS are presented. The natural frequencies obtained from the reference values are indicated with vertical lines. The CDFs of the percentage difference between F_n and F_{0n} are also presented in the figure. As can be observed, the range of the results is small and the influence of the random field $I(x)$ is not significant. The probability of the difference to be greater than 1% is 0.2 ($P((F_n - F_{0n})/F_{0n} \leq 1\%) = 0.2$) for the first three natural frequencies. This value indicates the small influence of $I(x)$ in the natural frequencies. The differences are negative due to the fact that all the simulated beams have knots and present a lengthwise decrease of $I(x)$ with respect to the adopted reference value I_0.

Influence of the uncertainty in the bending stiffness E(x)I(x) and mass density P in the natural frequencies

In this section, the propagation of the random field $E(x)I(x)$ and the random variable P in the first three natural frequencies F_n is evaluated. In a first stage, the mass

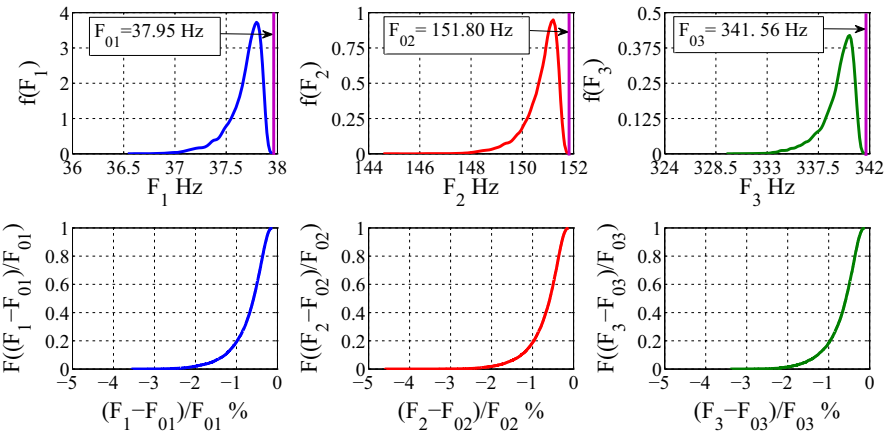

Fig. 3 Natural frequencies. Modal analysis with random field $I(x)$, PDFs of the first three natural frequencies F_n and CDFs of the percentage difference $F_n - F_{0n}$

density assumes a deterministic constant value along the beam. Then, the mass density assumes a random constant value along the beam adding a new source of uncertainty in the stochastic model. The reference values and the corresponding natural frequencies are the same as before.

The PDF of the first three natural frequencies and the CDFs of the percentage difference between F_n and F_{0n} obtained through the MCS are depicted in Fig. 4a, b (dotted and dashed lines plots). The results are found for the case of the bending stiffness modeled by a random field and the mass density by a deterministic value. The influence of the correlation length d adopted for the free-of-knots sections can be appreciated (d_1 dotted lines, d_∞ dashed lines). The PDFs of F_n have a same initial point in the zone of lower frequencies with both values of the correlation length and lead to frequencies with approximately the same probability. In this region, the beams have a larger amount of knots and the lengthwise variation of the MOE in the sections without knots is not relevant. From this initial point toward the upper percentiles of the $f[F_n]$ for the same probability, the values of F_n increase with

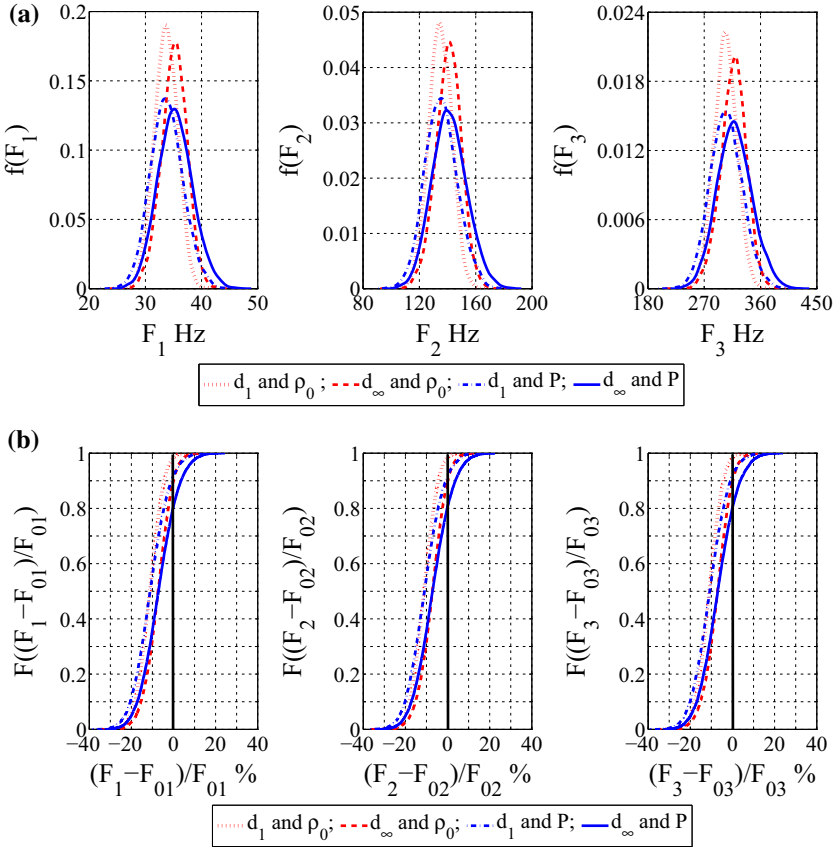

Fig. 4 Modal analysis with random field $E(x)I(x)$ and deterministic/random mass density. **a** PDFs of the first three natural vibration frequencies. **b** CDFs of the percentage difference $F_n - F_{0n}$

the increment of d. One possible interpretation of this result could be that the natural frequency of beams with higher stiffness and lower number of defects is located in this region and the values of d are more relevant for this case. Further, the introduction of the uncertainty in the MOE values enlarges the range of the response with respect to the results presented in the previous section. The range of the percentage difference is higher than the one obtained in the previous section as can be observed in Fig. 4b. This indicates that the influence of the random field $I(x)$ is negligible with respect to the influence of the random field $E(x)$. The differences are negative and positive due to the fact that the simulated beams can have higher values of $E(x)I(x)$ than the adopted homogeneous reference values of E_0I_0.

In what follows in this section, and in addition to the uncertain mechanical properties presented before, a random mass density (P in Eq. 3) is introduced. Figure 4a (dash-dot and solid lines plots) depicts the PDFs of the first three natural frequencies F_n, and Fig. 4b (dash-dot and solid lines plots) shows the CDFs of the percentage difference between F_n and F_{0n}. The influence of the random field $E(x)$ is simply appreciated in the shape of $f[F_n]$ that exhibits similar characteristics as described before (d_1 dash-dot lines, d_∞ solid lines). The range of percentage difference is higher than in the previous case (deterministic mass density). This indicates that the random variable P effect is not negligible. The differences are higher than the results presented in the previous section due to the fact that the relation $E(x)I(x)/P$ can adopt a larger range of values than the relation $E(x)I(x)/\rho_0$.

Statistics for the considered values of d and the two approaches employed for modeling the mass density in this section are depicted in Table 2. The mean value, SD and coefficient of variation of the random variable F_n are depicted. An increase of the value of d produces an increment in both the mean value and the SD of the random variable F_n. This means that a beam with homogeneous MOE in the free knots section presents higher values of natural frequency than a beam with non-homogeneous MOE in these sections. Further, they exhibit a larger dispersion from the expected value of F_n. The propagation of the mass density uncertainty is observed in the increment of the response range. This can be observed comparing the values of the SD $\sigma[F_n]$ when the mass density is modeled as either a deterministic value or a random variable. The coefficient of variation remains equal for the natural frequencies obtained with the corresponding value of d.

Table 2 Natural frequency modal analysis with the random field $E(x)I(x)$ and the random variable P, comparison between numerical results for the two values of d

Stochastic variables	Statistics	F_1		F_2		F_3	
		d_1	d_∞	d_1	d_∞	d_1	d_∞
$E(x)I(x)$	$E[F_n]$ Hz	33.64	35.09	134.77	140.58	303.74	316.57
	$\sigma[F_n]$ Hz	2.07	2.30	8.14	9.16	18.08	20.61
	σ/E	0.061	0.065	0.060	0.065	0.060	0.065
$E(x)I(x)$ and P	$E[F_n]$ Hz	33.81	35.31	135.50	141.34	305.27	318.45
	$\sigma[F_n]$ Hz	2.90	3.08	11.57	12.32	25.87	27.80
	σ/E	0.086	0.087	0.085	0.087	0.085	0.087

Alternatively, if the knot mass density were considered different to the clear wood value, then the mass density would be a stochastic field analogous to the MOE variable. However, the density was assumed constant within each beam, though variable among the different beams since the experimental evidence shows that no significant variations are found when *Eucalyptus grandis* is used.

Influence of the random fields I(x), E(x)I(x) and the random variable P in the mode shapes

Due to the stochastic variation of the mechanical properties of the beam in each section, the first three natural modes of vibration are represented by three stochastic processes parametrized by the position in the beam span x. The mean value and the SD functions ($E[\Phi_{F_n}(x)]$ and $\sigma[\Phi_{F_n}(x)]$) along the beam span of the first three stochastic processes $\Phi_{F_n}(x)$ are presented in Fig. 5 for the three cases of stochastic models studied in the previous section. In all cases, the SD function $\sigma[\Phi_{Fn}(x)]$ increases with the order of the natural vibration mode. More, the variation in the shape of the function $\sigma[\Phi_{F_n}(x)]$ for each natural mode can be observed. Similar results regarding the study of the natural frequencies and mode shapes of strings with randomly varying mass and stiffness have been presented by Manohar and Iyengar (1994). The mean value function is not modified by the values of the correlation length. Meanwhile, a decrease in the value of d produces an increment in the SD function $\sigma[\Phi_{F_n}(x)]$ (Fig. 5b, c). The shape of the function $\sigma[\Phi_{F_n}(x)]$ keeps approximately equal even though its values increase due to the addition of the MOE and mass density uncertainties. This behavior can be observed comparing Fig. 5b, c with Fig. 5a. The comparison of Fig. 5b, c shows that the function $\sigma[\Phi_{F_n}(x)]$ is slightly modified by the addition of the mass density uncertainty.

Buckling problem

Numerical results of the first three buckling loads P_n and modes Φ_{Pn} of a pinned-pinned *Eucalyptus grandis* timber column are reported in what follows. The parameters employed in the numerical simulation are the following: a column of length 2 m and with a nominal cross section 50 mm x 150 mm. The ratio of the length of the column to the lower cross-sectional dimension is equal to 40 (L/b = 40). This is equivalent to a slenderness of 139 (λ = 139). These geometrical parameters correspond to timber columns of structural size, which are often used in design practice.

Influence of the random field I(x) in the buckling load

In this section, the influence of the random field $I(x)$ in the first three buckling loads P_n is evaluated. The MOE assumes a deterministic constant value along the beam. The adopted reference values are the following: E_0 = 15.89 GPa and I_0 = 8.263×10^{-7} m^4. This I_0 value corresponds to a beam without knots. For these reference values and a column length L = 2 m, the first three buckling loads obtained

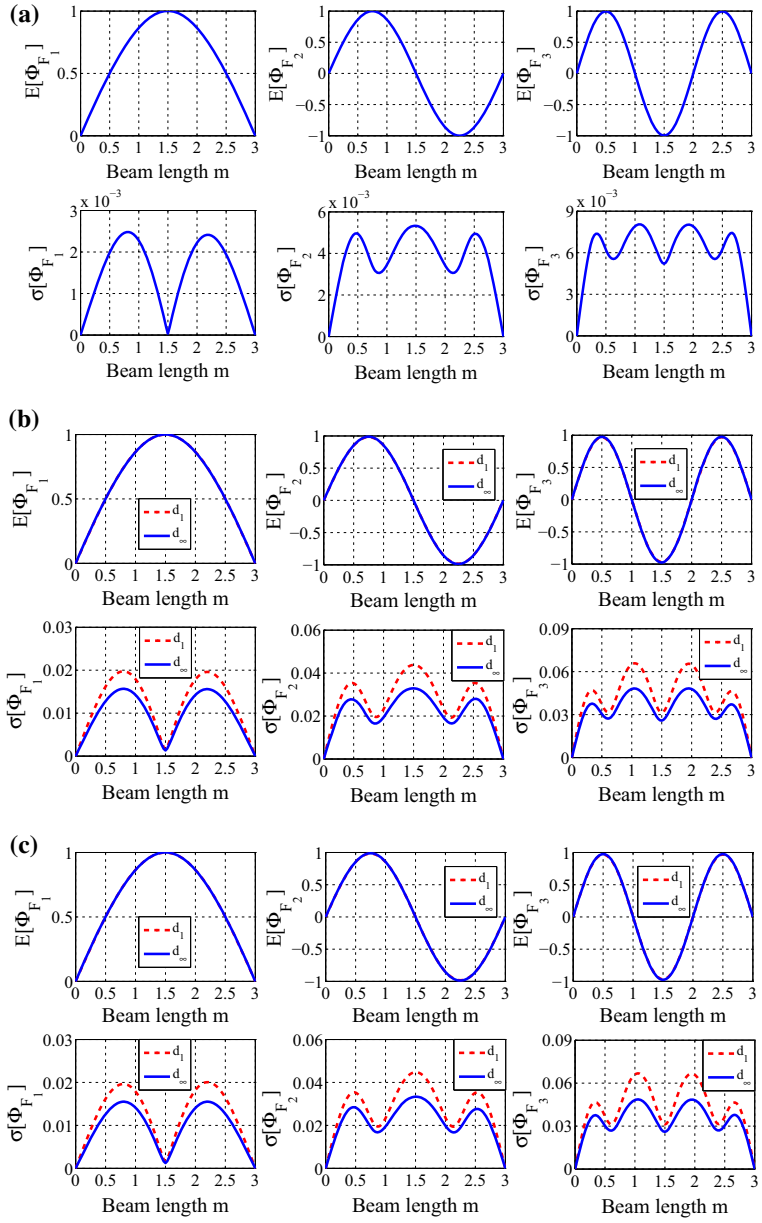

Fig. 5 Natural frequencies modal shapes. Mean value and SD functions ($E[\Phi_{F_n}(x)]$ and $\sigma[\Phi_{F_n}(x)]$) of the stochastic process $\Phi_{F_n}(x)$ (mode shape). **a** Random field $I(x)$. **b** Random field $E(x)I(x)$. **c** Random field $E(x)I(x)$ and random variable P

through the classical equation for a pinned-pinned column with homogeneous properties ($P_n = n^2\pi^2 E_0 I_0/L^2$) are P_{01} = 32.39 kN, P_{02} = 129.57 kN and P_{03} = 291.55 kN, respectively. The PDFs of the first three buckling loads obtained through

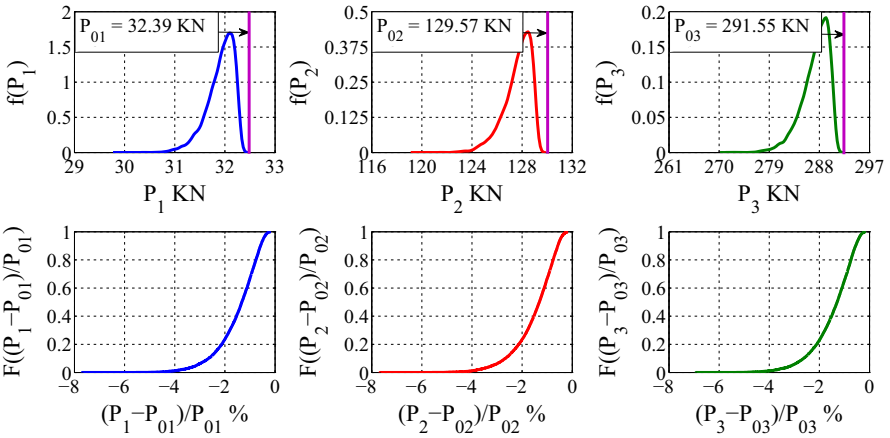

Fig. 6 PDFs of the first three buckling loads P_n and CDFs of the percentage difference $P_n - P_{0n}$ found with the random field $I(x)$

the MCS are presented in Fig. 6. The buckling loads obtained from the reference values are also indicated. The CDFs of the percentage difference between P_n and P_{0n} are depicted in the bottom plots.

The range of the results is small and the random field $I(x)$ effect is negligible. The probability of the difference to be greater than 2 % is 0.2 ($P((P_n - P_{0n})/P_{0n} \leq 2\,\%) = 0.2$) for the first three buckling loads indicating the low influence of $I(x)$ in the buckling load. The differences are negative due to the fact that all the simulated columns have knots and present a lengthwise decrease of $I(x)$ with respect to the adopted reference value I_0.

Influence of the uncertainty in the bending stiffness E(x)I(x) in the buckling load

The propagation of the random field $E(x)I(x)$ in the first three buckling loads P_n is reported herein. The reference values and the corresponding buckling loads are as before.

Figure 7 shows the PDFs of the first three buckling loads P_n (Fig. 7a) and the CDFs of the percentage difference between P_n and P_{0n} (Fig. 7b). The effect of the random field $E(x)$ is simply appreciated in the shape of $f[P_n]$ that presents the same characteristics described in the natural vibration problem section.

The range of the percentage difference is larger than the one obtained in the previous buckling case. This indicates that the variation due to the random field $I(x)$ is negligible compared to the influence of the random field $E(x)$. The differences are negative and positive due to the fact that the simulated beams can have higher values of $E(x)I(x)$ than the adopted homogeneous reference values of E_0I_0.

Table 3 includes the mean value, the SD and the coefficient of variation of the first three buckling loads for the considered values of correlation length. Like in the natural frequencies study, an increase of the value of d produces an increment in the

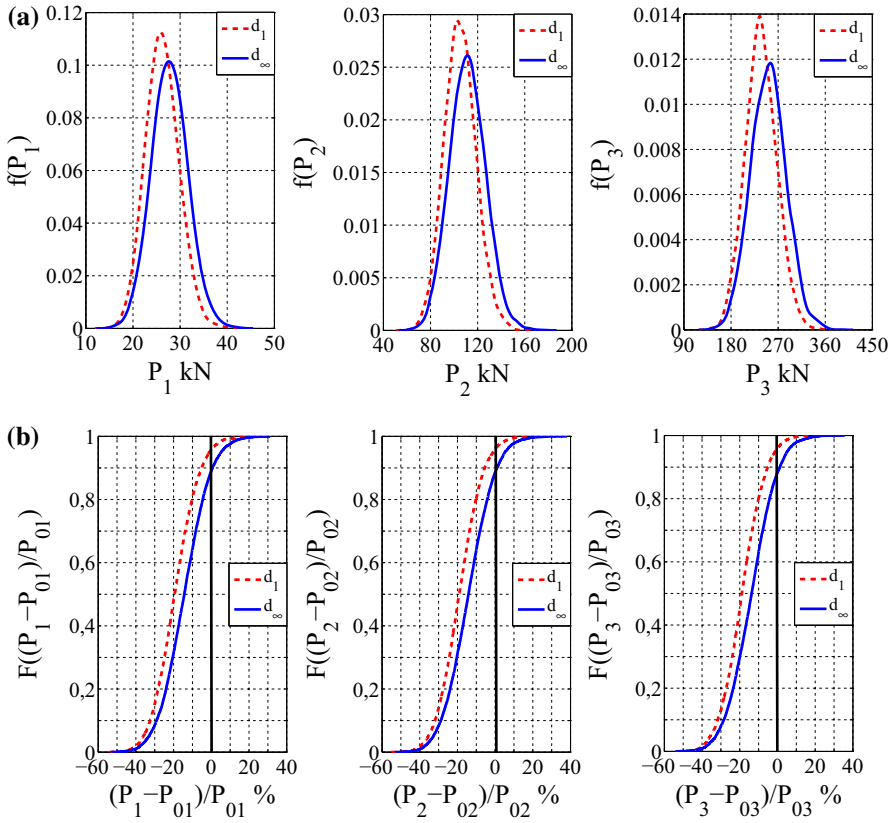

Fig. 7 Buckling problem with the random field $E(x)I(x)$. **a** PDFs of the first three buckling loads. **b** CDFs of the percentage difference $P_n - P_{0n}$

Table 3 Comparison between numerical results for the first three buckling loads and different values of d found with the random field $E(x)I(x)$

Statistics	P_1		P_2		P_3	
	d_1	d_∞	d_1	d_∞	d_1	d_∞
$E[P_n]$ kN	26.31	27.79	105.21	111.46	237.41	251.60
$\sigma[P_n]$ kN	3.36	3.79	13.50	15.15	30.06	33.77
σ/E	0.127	0.136	0.128	0.135	0.126	0.134

mean value and in the SD of the random variable P_n and the coefficient of variation remains constant for the buckling loads obtained with the corresponding value of d.

Influence of the random fields I(x) and E(x)I(x) in the buckling mode shapes

The mean value and the SD functions ($E[\Phi_{P_n}(x)]$ and $\sigma[\Phi_{P_n}(x)]$) along the column span of the first three stochastic processes of the mode shapes $\Phi_{P_n}(x)$ are presented

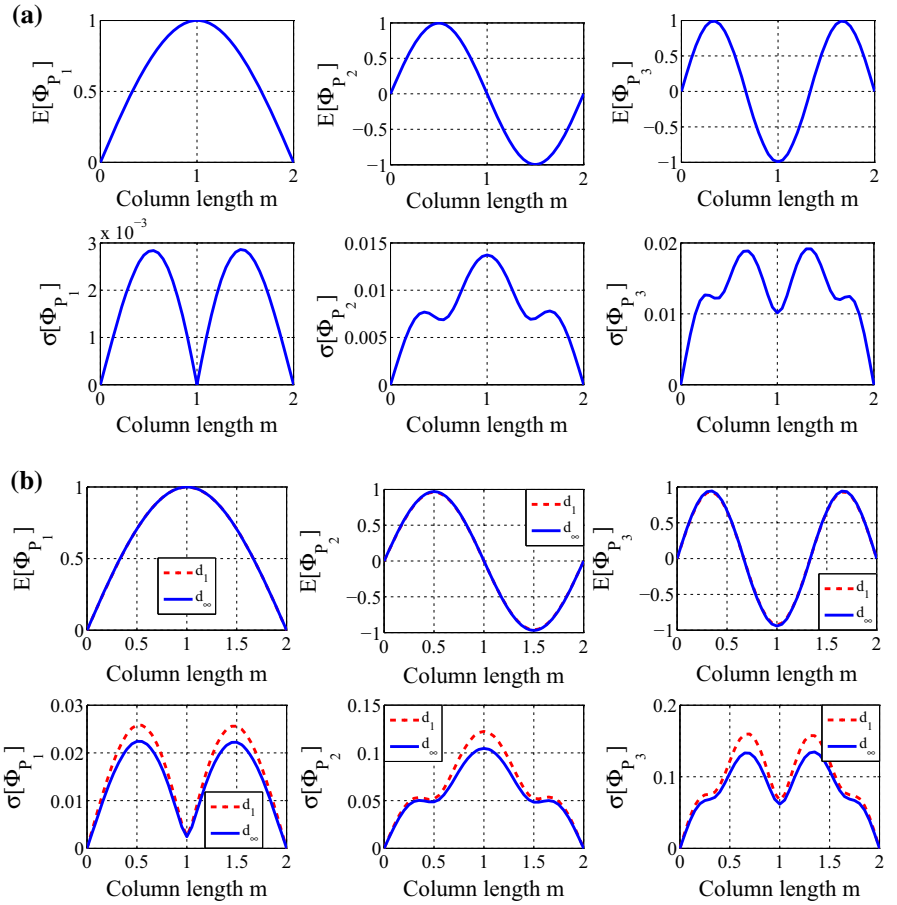

Fig. 8 Mean value and SD functions ($E[\Phi_{P_n}(x)]$ and $\sigma[\Phi_{P_n}(x)]$) of the stochastic process $\Phi_{P_n}(x)$ (mode shape). **a** Random field $I(x)$. **b** Random field $E(x)I(x)$

in Fig. 8 for the two previous cases of stochastic models of the buckling problem. The SD function $\sigma[\Phi_{P_n}(x)]$ increases with the order of the buckling mode. Further, the variation in the shape of the function $\sigma[\Phi_{P_n}(x)]$ for each buckling mode can be observed. In comparison with the results obtained for the natural vibration modes, the function $\sigma[\Phi_{P_n}(x)]$ has a different shape but shows a similar behavior when the order of the mode increases. In Fig. 8b, the mean value function is not modified by the values of the correlation length. Meanwhile, a decrease in the value of d produces an increment in the SD function $\sigma[\Phi_{P_n}(x)]$. The inhomogeneity of the MOE values in the free-of-knots sections produces a larger variation in the buckling modes. In addition, the shape of the function $\sigma[\Phi_{P_n}(x)]$ remains approximately equal even though its values increase due to the addition of the MOE uncertainty.

Conclusion

Sawn *Eucalyptus grandis* structural elements with uncertain material properties were studied, and in particular, the eigenvalues problems were analyzed in detail. A statistical study of the mechanical properties in the free vibration and buckling problems theory was carried out using the E–B beam theory.

The methodology included the SFEM and tools that permit to obtain a material structural properties approach which can represent closely the behavior of real timber elements. The traditional criterion of employing a normal PDF for the mechanical properties was addressed together with other alternatives, showing that the PDF that best fits the experimental results is the gamma distribution. The influence of the timber knots in the response is frequently disregarded. In the present study, its consideration derives in an improved representation of sawn timber structures. A model of the lengthwise variability of the Modulus of Elasticity (MOE) was presented starting from the weak-zone model to study the lengthwise variability of the bending strength. However, the present model introduced the presence of knots in the sectional parameters and the length of the weak zone in a different way.

The PDFs and CDFs of the first three natural frequencies and buckling loads in structural elements with uncertain material properties were obtained by MCS. The stochastic analysis yields further information on the structural components behavior. The influence in the response of the correlation length of the MOE of the free-of-knots sections was evaluated. If the CDF curves simulated for the two values of d are observed, it is possible to find that the lower correlation length (d_1) curve always yields higher values of probability for a given frequency. On the other hand, the homogeneous case (d_∞) leads to larger values of the SD. The validation of the numerical model was carried out using results of the experimental results of the first natural frequency. The length of the weak zones was calibrated, and it is shown that numerical simulations results with the MOE in the free-of-knots sections represented by a random field are closer to the experimental outcome, inasmuch as timber beams are of superior quality. The value of the correlation length was shown to be applicable to *Eucalyptus grandis* elements. The difference between numerical and experimental results is influenced by timber defects, such as the presence of pith, not included in the present numerical model.

The propagation of the mechanical parameters uncertainties in the natural frequencies and buckling loads was presented for different stochastic models. First, the influence of the random field of the second moment of area, $I(x)$, was studied. Then, the random field $E(x)I(x)$ was introduced with the correlation length (d) for the random field $E(x)$ in the beam free-of-knots sections. The increase in the value of the correlation length produces an increment in the SD of the response. Finally, for the free vibration problem, the mass density random variable P was added. The effect of the random field $I(x)$ is found to be negligible in comparison with the variability of the other mechanical properties. Consequently, the presence of the knots is more important regarding the MOE variability ($E(x)$) than in the variation of the second moment of the area ($I(x)$). The addition of the mass density

uncertainty through the random variable P increases the range of the response and slightly modifies the shape of the PDFs and CDFs found for the random field $E(x)I(x)$.

The free vibration and buckling mode shapes were also analyzed. Due to the stochasticity of the model, a random process parametrized by the position was obtained for both problems. The mean value remains equal in both problems, and it is not influenced by the stochastic parameters of the model. Meanwhile, the SD function changes its shape from one problem to the other. Also, the stochastic variation of the mechanical properties has an apparent effect. In general, the SD function increases its values from the first to the third natural frequency or buckling load and also due to the addition of uncertainty in the mechanical and physical parameters of the model.

The stochastic models introduced in the present study constitute a more realistic material approach, also feasible to be applied to reliability studies of serviceability limit states of structural components made of *Eucalyptus grandis* timber.

At present, the authors address the forced vibration problem in timber beams including a material damping model.

Acknowledgments The authors are grateful for the financial support of CONICET, SGCyT-UNS, MINCyT from Argentina and CAPES, CNPq and FAPERJ from Brazil. The experimental data provided by J.C. Piter and co-workers from FRCU-UTN (Argentina) are greatly acknowledged.

References

Baño V, Arriaga F, Soilán A, Guaita M (2011) Prediction of bending load capacity of timber beams using a finite element method simulation of knots and grain deviation. Biosyst Eng 109(4):241–249

Baño V, Argüelles-Bustillo R, Regueira R, Guaita M (2012) Determination of the stress-strain curve in specimens of Scots pine for numerical simulation of defect free beams. Materiales de construcción 62(306):269–284

Baño V, Arriaga F, Guaita M (2013) Determination of the influence of size and position of knots on load capacity and stress distribution in timber beams of Pinus sylvestris using finite element model. Biosyst Eng 114(3):214–222

Bathe KJ (1982) Finite element procedures in engineering analysis. Prentice-Hall, New Jersey

Benjamin RJ, Cornell CA (1970) Probability, statistics and decision for civil engineers. McGraw-Hill, New York

CIRSOC 601 (2013) Argentinean standard of timber structures (In Spanish). Instituto Nacional de Tecnología Industrial (INTI)- Centro de Investigación de los Reglamentos Nacionales de Seguridad para las Obras Civiles (CIRSOC), Buenos Aires

Czmoch I (1998) Influence of structural timber variability on reliability and damage tolerance of timber beams. PhD thesis, Luleå Tekniska Universitet, Luleå

Der Kiureghian A, Ke JB (1988) The stochastic finite element method in structural reliability. Probab Eng Mech 3(2):83–91

Der Kiureghian A, Liu PL (1986) Structural reliability under incomplete probability information. J Eng Mech ASCE 112:85–104

Ditlevsen O, Madsen HO (1996) Structural reliability methods. Wiley, Chichester

EN 338 (1996) Structural timber. Strength classes (In Spanish). AENOR-Asociación Española de Normalización y Certificación, Madrid

EN 408 (1996) Timber structures. Structural timber and glued laminated timber. Determination of some physical and mechanical properties (In Spanish). AENOR-Asociación Española de Normalización y Certificación, Madrid

García D, Piter J, Escalante M, Rosales M (2013) Structural behavior of timber beams with a modulus of elasticity represented by a random field. Mecánica Computacional 32(15):631–645

Ghanem RG, Spanos PD (1991) Stochastic finite elements: a spectral approach. Springer, New York
Guindos P, Guaita M (2013) A three-dimensional wood material model to simulate the behavior of wood with any type of knot at the macro-scale. Wood Sci Technol 47(3):585–599
Guindos P, Guaita M (2014) The analytical influence of all types of knots on bending. Wood Sci Technol 48(3):533–552
INTA (1995) Manual for producers of eucalyptus of the Argentinean Mesopotamia (In Spanish). Forestry Group, National Institute of Technology for Farming, EEA Concordia, Argentina
IRAM 9662-2 (2006) Glued laminated timber. Visual strength grading of boards, part 2: boards of Eucalyptus grandis (In Spanish). Argentinean Institute for Standardization and Certification (IRAM), Buenos Aires
Isaksson T (1999) Modeling the variability of bending strength in structural timber: length and load configuration effects. PhD thesis, Lund Institute of Technology, Lund
Kline DE, Woeste FE, Bendtsen B (1986) Stochastic model for modulus of elasticity of lumber. Wood Fiber Sci 18(2):228–238
Köhler J (2007) Reliability of timber structures. PhD thesis, Swiss Federal Institute of Technology, Zürich
Köhler J, Sørensen JD, Faber MH (2007) Probabilistic modeling of timber structures. Struct Saf 29(4):255–267
Lukacevic M, Füssl J (2014) Numerical simulation tool for wooden boards with a physically based approach to identify structural failure. Eur J Wood Prod 72(4):497–508
Manohar C, Iyengar R (1994) Free vibration analysis of stochastic strings. J Sound Vib 176(1):35–48
Melchers RE (1999) Structural reliability: analysis and prediction. Wiley, New York
Piter J (2003) Strength grading of sawn timber as structural material: development of a method for the Argentinean Eucalyptus grandis (In Spanish). PhD thesis, Universidad Nacional de la Plata, La Plata
Piter J, Zerbino R, Blass H (2004) Visual strength grading of Argentinean Eucalyptus grandis. Holz Roh Werkst 62(1):1–8
Rubinstein RY, Kroese DP (2007) Simulation and the Monte Carlo method, 2nd edn. Wiley, New Jersey
SBN 1980 (1981) Swedish Building Code (In Swedish). National Swedish Board of Physical Planning and Building, Stockholm
Shannon C (1948) A mathematical theory of communication. Bell Syst Technol J 27:379–423